# Electric Dipole Moments in a General Two-Higgs Doublet Model

*Sven Teunissen*

*Advisor: Wei-Shu Hou*

*Graduate Institute of Physics*

*National Taiwan University*

*Taipei, Taiwan*

June 2024

# Abstract

The Standard Model (SM) of particle physics has been the dominant theory of all fundamental physics sans gravity for a good 50-or-so years. The SM provides a unifying mathematical framework, explanations for various atomic and subatomic phenomena, and a plethora of predictions, many of which have since been verified by experiments to high precision. Nevertheless, there are still questions the SM still does not have an answer for, one of them being the imbalance of naturally existing matter and antimatter, also known as the Baryon Asymmetry of the Universe (BAU). Motivated by this question (among others), there have been various theoretical attempts at extending beyond the Standard Model (BSM). One family of these extensions are the Two-Higgs Doublet Models (2HDMs), which propose an extra Higgs doublet with varying properties. Among these 2HDMs, one type does not have any assumed symmetry or coupling constraints, and is known as the General Two Higgs Doublet Model (G2HDM). A key feature of such theories attempting to address BAU is large charge-parity violation (CPV). On the experimental front, both the lack of new collider observations as well as the smallness of low-energy precision measurements put heavy constraints on BSM CPV. In particular, the electric dipole moments (EDMs) of various fundamental particles provide a *litmus test* for CPV effects. This study is an examination and analysis of various EDMs under the G2HDM framework. We start with the electron EDM (eEDM), introducing a *cancellation mechanism* that allows for an adequate parameter space to address the BAU issue while evading the current EDM bounds. We then extend the framework to the muon and the tau, and present both general

and cancellation-imposed results for the EDM of heavier leptons. We also probe the effects of the light quark EDMs through the neutron EDM (nEDM), taking into account gluon-related contributions. At last, we present a combined scenario analysis of the eEDM and the nEDM, signifying that experimental verification, or even *discovery*, is achieveable within the next decade or two.

# Contents

**Abstract** i

**List of Figures** v

**List of Tables** vii

**1 Introduction** 1

1.1 The Standard Model of Particle Physics . . . . . 1

1.2 Limits of the Standard Model . . . . . 1

**2 The General Two-Higgs Doublet Model** 3

**3 Electric Dipole Moment** 5

3.1 The electric dipole moment in particle physics . . . . . 5

3.1.1 The Dirac method . . . . . 6

3.1.2 Form factor decomposition . . . . . 7

3.1.3 General properties of EDM . . . . . 8

3.2 G2HDM contributions to EDMs . . . . . 8

3.2.1 One-loop v.s. Two-loop . . . . . 8

3.2.2 Two-loop Formulae . . . . . 9

3.3 Chromoelectric dipole moment . . . . . 12

**4 Electric Dipole Moment of Leptons** 17

4.1 Experimental Overview . . . . . 17

4.2 The Electron . . . . . 18
4.2.1 Cancellation Mechanism . . . . . 18
4.2.2 Enlarging the Parameter Space . . . . . 19
4.3 The Muon . . . . . 21
4.4 The Tau Lepton . . . . . 21

**5 Electric and Chromo-electric Dipole Moment of Quarks 25**

**6 Conclusion 31**
6.1 Comments . . . . . 31
6.1.1 Heavy Higgs Masses . . . . . 31
6.1.2 Muon $g-2$ . . . . . 32
6.1.3 Top Chromo-EDM . . . . . 32
6.2 Summary and Conclusion . . . . . 33

**Reference 35**

# List of Figures


3.1 One-loop diagram . . . . . 10

3.2 Two-loop Barr-Zee diagram . . . . . 10

3.3 Specific Two-loop Barr-Zee diagrams . . . . . 14

3.4 Diagrams relevant to chromo-EDM . . . . . 15

4.1 eEDM v.s. $r$ for a larger range of $\rho_{tt}$ with ansatz Eq. (4.5). ($c_\gamma = 0.1, m_{H,A,H^+} = 500\,\text{GeV}$) . . . . . 20

4.2 $\mu$EDM results. . . . . 22

4.3 $\tau$EDM results. . . . . 22

5.1 nEDM experimental progress [**?**] . . . . . 27

5.2 nEDM results. . . . . 27

5.3 Combined eEDM-nEDM result. . . . . 27

5.4 Results for eEDM and nEDM with $|\rho_{uu}| \sim \lambda_u$. . . . . 29

# List of Tables

# Chapter 1

# Introduction

One of the biggest unanswered questions of particle physics is that of baryogenesis. Specifically, if electroweak baryogenesis (EWBG) [**?**] were to occur, one would require very large CP violation (CPV) beyond the Standard Model (BSM), since the SM currently houses all its CPV in the CKM matrix [**?**]. However, such large BSM-CPV should have led to new discoveries at the LHC, which evidently is *not* what has been observed. Moreover, in the low-energy precision frontier, electric diploe moments (EDMs) provide a *litmus test* for CPV effects, and experiments have achieved higher and higher precision without discoveries, setting ever more stringent bounds.

## 1.1 The Standard Model of Particle Physics

The current working theory in the realm of particle physics is the Standard Model (SM).

## 1.2 Limits of the Standard Model

The SM is a powerful theory, providing a unifying framework for three of the four fundamental forces, and producing many verified predictions. To quote from the

textbook *Modern Particle Physics* by Mark Thomson [**?**], "[The Standard Model] is a model constructed from a number of beautiful and profound theoretical ideas put together in a somewhat *ad hoc* fashion in order to reproduce the experimental data." However, amidst all its strength, there are still several open questions that the SM has not been able to answer.

# Chapter 2

# The General Two-Higgs Doublet Model

Following Gell-Mann's *Totalitaian principle*, as a natural extension to the SM, we can introduce a second Higgs doublet. This second doublet couples to all flavors and families of fermions, and has no symmetry requirement imposed upon it. Hence, it is referred to as the "General Two Higgs Doublet Model", or G2HDM for short.

The G2HDM Lagrangian can be written as [**?**, **?**]

$$\mathcal{L} = -\frac{1}{\sqrt{2}} \sum_{f=u,d,\ell} \bar{f}_i \Big[ \Big( -\lambda_i^f \delta_{ij} s_\gamma + \rho_{ij}^f c_\gamma \Big) h + \Big( \lambda_i^f \delta_{ij} c_\gamma + \rho_{ij}^f s_\gamma \Big) H - i\,\mathrm{sgn}(Q_f) \rho_{ij}^f A \Big] R\, f_j$$
$$- \bar{u}_i \left[ (V\rho^d)_{ij} R - (\rho^{u\dagger} V)_{ij} L \right] d_j H^+ - \bar{\nu}_i \rho_{ij}^L R\, \ell_j H^+ + \mathrm{h.c.}, \tag{2.1}$$

where the generation indices $i$, $j$ are summed over, $L$, $R = (1 \pm \gamma_5)/2$ are projections, $V$ is the CKM matrix for quarks and unity for leptons. $\lambda^f$ are the SM Yukawa matrices, and $\rho^f$ are the extra-Yukawa matrices. A key takeaway is that each family of fermions (u-type, d-type, lepton) is associated with its own extra-Yukawa $\rho$ matrix. In this scenario, flavor-changing neutral Higgs (FCNH) processes are controlled by *flavor hierarchies* and *alignment*. Flavor hierarchies means that the $\rho$ matrices somehow "know" the current flavor structure of the SM,

represented by the "rule of thumb" [**?**]

$$\rho_{ii} \lesssim \mathcal{O}(\lambda_i), \quad \rho_{1i} \lesssim \mathcal{O}(\lambda_1), \quad \rho_{3j} \lesssim \mathcal{O}(\lambda_3), \tag{2.2}$$

with $j \neq 1$. Alignment means that $c_\gamma \equiv \cos\gamma = \cos(\beta - \alpha)$ is small. Consequently, the SM-like Higgs $h$ is mostly controlled by the SM Yukawas, while the newly introduced $\rho$ matrices control the exotic Higgses $H, A, H^\pm$. A remarkable feature of G2HDM is that $\mathcal{O}(1)$ $\rho_{tt}$ can drive EWBG through [**?**] $\lambda_t \mathrm{Im}\rho_{tt}$.

# Chapter 3

# Electric Dipole Moment

## 3.1 The electric dipole moment in particle physics

Classically, the electric dipole moment of a charge distribution is found as the coefficient of the $l = 1$ term in the multipole expansion of the potential of said distribution. Explicitly, it is[1]

$$\mathbf{d} = \int (\mathbf{r} - \mathbf{r}_0)\rho(\mathbf{r})\,\mathrm{d}^3\mathbf{r} \tag{3.1}$$

with $\mathbf{r}_0$ the center of mass of the charge distribution [**?**, **?**]. It is related to the seperation of charges or nonuniformity along a single axis in the charge distribution; for a distribution of nonzero net charge, it is also related to the position of the center of mass with respect to the origin. It is inherently a property of systems of finite size[2]. However, in particle physics, we are not dealing with composite systems, but the properties of the fundamental particles. That means we are instead looking for an *intrinsic* EDM of point-like particles that is attributed to the particle itself, and not a seperation of charges. This is analogous to the (spin) magnetic dipole moment being an *intrinsic* property and not a tiny loop of current. In particluar,

[1] In classical texts, the dipole moment is represented with the symbol $\mathbf{p}$. For the sake of consistency with the particle physics notation, I have chosen the symbol $\mathbf{d}$ instead.

[2] There are point-like "dipoles" etc. in the classical framework, but they are purely mathematical and are not attributed to any physical thing.

particle physicists are interested in the EDMs of various fermions, since they are the point-like building blocks of all matter. Generally speaking, there are two ways to introduce this "EDM term", approaching the issue from slightly different angles.

### 3.1.1 The Dirac method

The first method is that of Dirac [**?**]. In his 1928 paper, which gave birth to his famous Dirac equation, he also wrote down the equation for the electron in an arbitrary electromagnetic field. Adapted into more modern notation, it is written as

$$[-(E - e\phi) + \boldsymbol{\alpha} \cdot (\mathbf{p} - e\mathbf{A}) + \beta m]\, \psi = 0 \tag{3.2}$$

where

$$\alpha_i = \gamma^5 \Sigma_i = \begin{pmatrix} 0 & I \\ I & 0 \end{pmatrix} \begin{pmatrix} \sigma_i & 0 \\ 0 & \sigma_i \end{pmatrix} = \begin{pmatrix} 0 & \sigma_i \\ \sigma_i & 0 \end{pmatrix}, \quad \beta = \begin{pmatrix} I & 0 \\ 0 & -I \end{pmatrix} \tag{3.3}$$

in the Pauli-Dirac representation. By "squaring" (3.2) one obtains

$$\begin{aligned} &[(E - e\phi) + \boldsymbol{\alpha} \cdot (\mathbf{p} - e\mathbf{A}) + \beta m]\, [-(E - e\phi) + \boldsymbol{\alpha} \cdot (\mathbf{p} - e\mathbf{A}) + \beta m]\, \psi = 0 \\ \Longrightarrow\ &\Big[-(E - e\phi)^2 + (\boldsymbol{\Sigma} \cdot (\mathbf{p} - e\mathbf{A}))^2 + m^2 \\ &\quad + \gamma^5 \left\{(E - e\phi)(\boldsymbol{\Sigma} \cdot (\mathbf{p} - e\mathbf{A})) - (\boldsymbol{\Sigma} \cdot (\mathbf{p} - e\mathbf{A}))(E - e\phi)\right\}\Big]\, \psi = 0 \end{aligned} \tag{3.4}$$

After some matrix algebra, in particular $(\boldsymbol{\Sigma} \cdot \mathbf{a})(\boldsymbol{\Sigma} \cdot \mathbf{b}) = (\mathbf{a} \cdot \mathbf{b})I + i\boldsymbol{\Sigma} \cdot (\mathbf{a} \times \mathbf{b})$, and casting $E$ and $\mathbf{p}$ back into their operator forms when necessary, we arrive at

$$\Big[-(E - e\phi)^2 + (\mathbf{p} - e\mathbf{A})^2 + m^2 - e\boldsymbol{\Sigma} \cdot \mathbf{B} - ie\gamma^5 \boldsymbol{\Sigma} \cdot \mathbf{E}\Big]\, \psi = 0 \tag{3.5}$$

which introduces two additional terms, corresponding to the magnetic and the electric dipole moment of the electron, respectively. At the time, Dirac thought the EDM term was merely a consequence of the "squaring" used in the derivation arbitrarily introducing an imaginary term from a real Hamiltonian, and disregarded it. It was only until 1958 when Salpeter [**?**] reintroduced this term in an "interaction Lagrangian" point of view.

### 3.1.2 Form factor decomposition

The second method is based on form factor decomposition. This method was recently seen in [**?**]. We start by expressing the expectation value of the electromagnetic 4-current in momentum space as

$$\langle p_f|j^\mu|p_i\rangle = \bar{u}(\mathbf{p_f})\mathcal{O}^\mu(l,q)u(\mathbf{p_i}) \tag{3.6}$$

where $l \equiv p_f + p_i$ is the total 4-momentum, $q \equiv p_f - p_i$ is the momentum transfer, and $\mathcal{O}^\mu(l,q)$ is an operator whose matrix element between the spinors is a Lorentz vector. We then want to decompose $\mathcal{O}^\mu(l,q)$ in terms of the Clifford algebra of the Dirac gamma matrices. After identifying all possible combinations and contractions of $\left\{q^\mu, l^\mu, \gamma^\mu, \gamma^5, \sigma^{\mu\nu}, \epsilon^{\mu\nu\alpha\beta}\right\}$, applying various Gordon-like identities, and imposing gauge invariance[3] $q_\mu j^\mu = 0$, we arrive at four independent terms

$$\begin{aligned}
&\bar{u}(\mathbf{p_f})\mathcal{O}^\mu(l,q)u(\mathbf{p_i}) \\
&= \bar{u}(\mathbf{p_f})\left\{F_1(q^2)\gamma^\mu + \frac{i\sigma^{\mu\nu}}{2m}q_\nu F_2(q^2)\right. \\
&\qquad \left. +(-\gamma^5\sigma^{\mu\nu}q_\nu)\frac{1}{4m}F_3(q^2) + \frac{1}{2m}\left(q^\mu - \frac{q^2}{2m}\gamma^\mu\gamma^5\right)F_4(q^2)\right\}u(\mathbf{p_i})
\end{aligned} \tag{3.7}$$

We then couple this with the electromagnetic potential $A_\mu$ to obtain some physical insight on this result. Taking the non-relativistic limit ($q^2 = 0$), we can identify

$$F_1(0) = Q, \quad \frac{1}{2m}\left(F_1(0) + F_2(2)\right) = \mu, \quad -\frac{1}{2m}F_3(0) = d \tag{3.8}$$

are the charge, magnetic dipole moment, and electric dipole moment, respectively. Transforming the coupled current plus EM field back into position space, we can obtain the addition to the interaction Lagranginan for each term as well.

[3] Note that without gauge invariance imposed, there ought to be six independent terms, which is the case for the Weak current.

### 3.1.3 General properties of EDM

Regardless of approach, the end result, in terms of quantum field theory, is the inclusion of an effective dimension-5 interaction operator to the EM Lagrangian,

$$-\frac{i}{2}d_f\left(\bar{f}\sigma^{\mu\nu}\gamma_5 f\right)F_{\mu\nu}. \tag{3.9}$$

that produces EDM $d_f$ for a fermion $f$, where $F_{\mu\nu}$ is the electromagnetic field strength tensor. If we examine the EDM term under the lens of discrete symmetry transformations, we can see that

$$\begin{aligned} \mathbf{E} &\xrightarrow{P} -\mathbf{E} & \mathbf{E} &\xrightarrow{T} \mathbf{E} \\ \mathbf{\Sigma} &\xrightarrow{P} \mathbf{\Sigma} & \mathbf{\Sigma} &\xrightarrow{T} -\mathbf{\Sigma} \end{aligned} \tag{3.10}$$

for parity transformation $P$ and time-reversal transformation $T$. Thus, a nonzero EDM of fundamental particles indicates that both time-reversal and parity invariance are broken.

## 3.2 G2HDM contributions to EDMs

### 3.2.1 One-loop v.s. Two-loop

In G2HDM, the first finite contribution to EDM appears at one-loop (Figure 3.1). If we look at the figure, there are two Yukawa interaction vertices along the fermion line. Each Yukawa interaction vertex flips the chirality of the fermion. In the previous section we observed that the dipole operator breaks parity invariance, and thus is chirality violating. Since the only chirality-flipping vertices along the fermion line are the Yukawa interaction vertices, we need an extra chirality flip somewhere along the line to obtain the correct chiral structure. This is achieved by requiring an additional mass insertion on the fermion line, i.e. treating the small mass of the fermion as an "interaction" between the (massless) chiral states. Since the mass of the fermions in question are very small, both the Yukawa vertices and the mass insertion effectively suppress the amplitude of the one loop-diagrams.

This is known as “chiral suppression”, and opens the possibility of two-loop diagrams making meaningful contributions.

A certain set of two-loop diagrams, known as Barr-Zee diagrams (Figure 3.2), are indeed of importance. These diagrams were first mentioned by Bjorken and Weinberg [**?**], but it was Barr and Zee [**?**] that calculated neutral scalar contributions with top quark and gauge bosons in the loop. This was later extended [**?**, **?**, **?**, **?**, **?**] to include other two-loop diagrams. These diagrams only contain one Yukawa interaction vertex, hence one chirality flip, as opposed to three in the one-loop case. The relative enhancement due to the lack of the two mass factors more than compensate for the suppression from the additional loop factor. Thus, interestingly, the two-loop diagrams become the dominant contribution to the EDM interaction operator.

### 3.2.2 Two-loop Formulae

In this subsection, we list all the relevant formulae involved in the calculation of the two-loop Barr-Zee diagram amplitudes with different loop particles. The formulae are compiled from various resources, and verified by us before using them. We also explicitly draw out all of the corresponding diagrams in Figure 3.3. The formulae for the neutral-Higgs-mediated diagrams are taken from [**?**]; The formulae for the charged-Higgs-mediated diagrams are taken from [**?**]. The notation follows that of [**?**].

$$(d_l^{\phi G})_t = -\frac{e\, m_l}{(4\pi)^4}\sqrt{2}G_F \sum_{\phi=h,H,A}\sum_{G=\gamma,Z} N_c Q_t (g^L_{Gll} + g^R_{Gll}) \times \left[\frac{g^A_{\phi ll}}{m_l/v}\frac{g^V_{\phi tt}}{m_t/v}\mathcal{I}_1^G(m_t, m_\phi) + \frac{g^V_{\phi ll}}{m_l/v}\frac{g^A_{\phi tt}}{m_t/v}\mathcal{I}_2^G(m_t, m_\phi)\right] \quad (3.11)$$

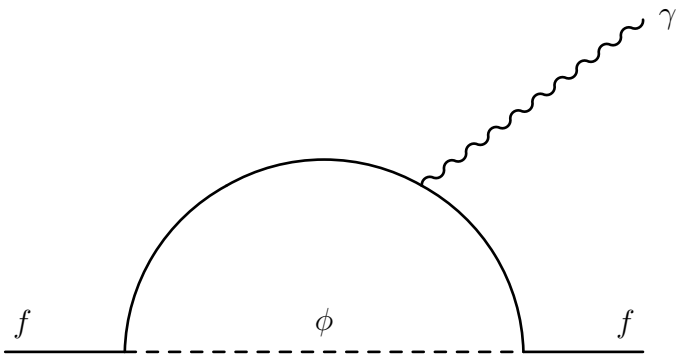


Figure 3.1: One-loop diagram

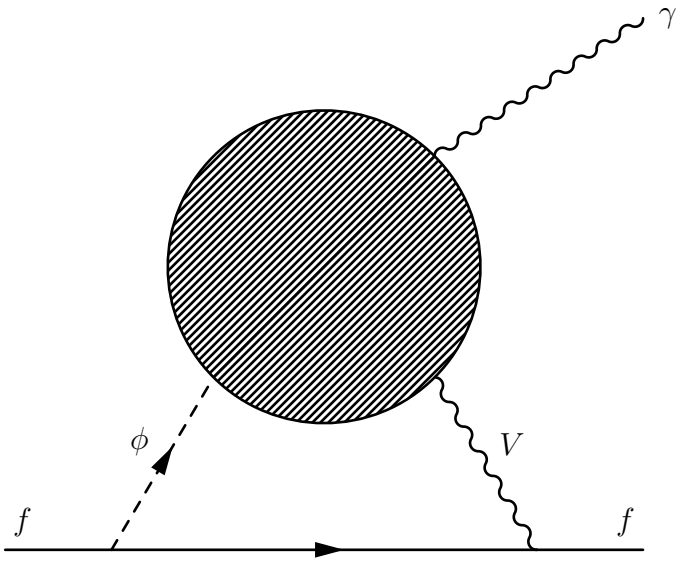


Figure 3.2: Two-loop Barr-Zee diagram

where

$$\mathcal{I}_1^G(m_t,m_\phi)=(g_{Gtt}^L+g_{Gtt}^A)\frac{m_t^2}{m_\phi^2-m_G^2}\left(-2\frac{m_G^2}{m_t^2}f\left(\frac{m_t^2}{m_G^2}\right)+2\frac{m_\phi^2}{m_t^2}f\left(\frac{m_t^2}{m_\phi^2}\right)\right)$$
$$\mathcal{I}_2^G(m_t,m_\phi)=(g_{Gtt}^L+g_{Gtt}^A)\frac{m_t^2}{m_\phi^2-m_G^2}\left(-2\frac{m_G^2}{m_t^2}g\left(\frac{m_t^2}{m_G^2}\right)+2\frac{m_\phi^2}{m_t^2}g\left(\frac{m_t^2}{m_\phi^2}\right)\right) \tag{3.12}$$

$$(d_l^{\phi G})_W=+\frac{e\,m_l}{(4\pi)^4}\sqrt{2}G_F\sum_{\phi=h,H,A}\sum_{G=\gamma,Z}(g_{Gll}^L+g_{Gll}^R)\frac{g_{\phi ll}^A}{m_l/v}\frac{g_{WW\phi}}{2m_W^2/v}\mathcal{I}_W^G(m_\phi) \tag{3.13}$$

where

$$\begin{aligned}\mathcal{I}_W^G(m_\phi)=&g_{WWG}\frac{2m_W^2}{m_\phi^2-m_G^2}\\&\times\left[-\frac{1}{4}\left\{\left(6-\frac{m_G^2}{m_W^2}\right)+\left(1-\frac{m_G^2}{2m_W^2}\right)\frac{m_\phi^2}{m_W^2}\right\}\left[-2\frac{m_\phi^2}{m_W^2}f\left(\frac{m_W^2}{m_\phi^2}\right)+2\frac{m_G^2}{m_W^2}f\left(\frac{m_W^2}{m_G^2}\right)\right]\right.\\&\left.+\left\{\left(-4+\frac{m_G^2}{m_W^2}\right)+\frac{1}{4}\left(\left(6-\frac{m_G^2}{m_W^2}\right)+\left(1-\frac{m_G^2}{2m_W^2}\right)\frac{m_\phi^2}{m_W^2}\right)\right\}\left[-2\frac{m_\phi^2}{m_W^2}g\left(\frac{m_W^2}{m_\phi^2}\right)+2\frac{m_G^2}{m_W^2}\right.\right.\end{aligned} \tag{3.14}$$

$$(d_l^{\phi G})_{H^\pm}=+\frac{e\,m_l}{(4\pi)^4}\sqrt{2}G_F\sum_{\phi=h,H,A}\sum_{G=\gamma,Z}(g_{Gll}^L+g_{Gll}^R)\frac{g_{\phi ll}^A}{m_l/v}\frac{g_{\phi H^+H^-}}{v}\mathcal{I}_3^G(m_{H^\pm},m_\phi) \tag{3.15}$$

where

$$\begin{aligned}\mathcal{I}_3^G(m_{H^\pm},m_\phi)=&-\frac{1}{2}g_{GH^+H^-}\frac{v^2}{m_\phi^2-m_G^2}\\&\times\left[\left(-2\frac{m_G^2}{m_{H^\pm}^2}f\left(\frac{m_{H^\pm}^2}{m_G^2}\right)+2\frac{m_\phi^2}{m_{H^\pm}^2}f\left(\frac{m_{H^\pm}^2}{m_\phi^2}\right)\right)-\left(-2\frac{m_G^2}{m_{H^\pm}^2}g\left(\frac{m_{H^\pm}^2}{m_G^2}\right)+2\frac{m_\phi^2}{m_{H^\pm}^2}g\left(\frac{m}{r}\right.\right.\right.\end{aligned} \tag{3.16}$$

$$(d_l^{H^+W^+})_{t/b}= \tag{3.17}$$

$$(d_l^{H^+W^+})_W= \tag{3.18}$$

$$(d_l^{H^+W^+})_{H^+} = \tag{3.19}$$

with loop functions

$$\begin{aligned} f(a) &= \frac{1}{2}a\int_0^1 \mathrm{d}z\, \frac{1-2z(1-z)}{z(1-z)-a}\log\frac{z(1-z)}{a} \\ g(a) &= \frac{1}{2}a\int_0^1 \mathrm{d}z\, \frac{1}{z(1-z)-a}\log\frac{z(1-z)}{a} \end{aligned} \tag{3.20}$$

$$\begin{aligned} T(a) &= \\ B(a) &= \end{aligned} \tag{3.21}$$

## 3.3 Chromoelectric dipole moment

If we were only interested in lepton EDM, then the previous discussion would have been sufficient, since leptons only participate in the electroweak interaction. However, quarks also participate in the strong interaction, so there will be QCD-related effects. This can be found in two additional terms in the Lagrangian: the chromo-EDM $\tilde{d}_f$ for fermion $f$, and the Weinberg term $C_W$ for gluon interactions [**?**], written as

$$-\frac{ig_s}{2}\tilde{d}_f\left(\bar{f}\sigma^{\mu\nu}T^a\gamma_5 f\right)G^a_{\mu\nu} \qquad\qquad -\frac{1}{3}C_W f^{abc}G^a_{\mu\sigma}G^{b,\sigma}_{\nu}\tilde{G}^{c,\mu\nu} \tag{3.22}$$

which correspond to the diagrams in Figure 3.4. The chromo-EDM term is essentially when the vector bosons of the "ordinary" EDM interaction are replaced by gluons instead. Since only quarks interact with gluons, only the diagram with a fermion loop remains. The Weinberg term is relevant because quarks always exist in bound hadronic states. That means experimentally we use the EDM of hadrons to infer about quark EDM, and thus the gluon interactions within the hadrons will contribute to the hadron EDM. The formulae for calculating the cEDM are

$$\tilde{d}_f = +\frac{m_f}{(4\pi)^4}\sqrt{2}G_F \sum_{\phi=h,H,A} 2g_s^2 \frac{m_f^2}{m_\phi^2}\left[\frac{g^A_{\phi ff}}{m_f/v}\frac{g^V_{\phi tt}}{m_t/v}\left(-2\frac{m_\phi^2}{m_t^2}f\left(\frac{m_t^2}{m_\phi^2}\right)\right)+\frac{g^V_{\phi ff}}{m_f/v}\frac{g^A_{\phi tt}}{m_t/v}\left(-2\frac{m_\phi^2}{m_t^2}g\left(\frac{m_t^2}{m_\phi^2}\right)\right)\right. \tag{3.23}$$

$$C_W = \tag{3.24}$$

The contribution of the Weinberg diagram can be evaluated using QCD running.

$$\frac{d_f(\mu_h)}{2} = \tag{3.25}$$

$$\frac{\tilde{d}_f(\mu_h)}{2} = \tag{3.26}$$

$$C_W(\mu_h) = \tag{3.27}$$

where constants.

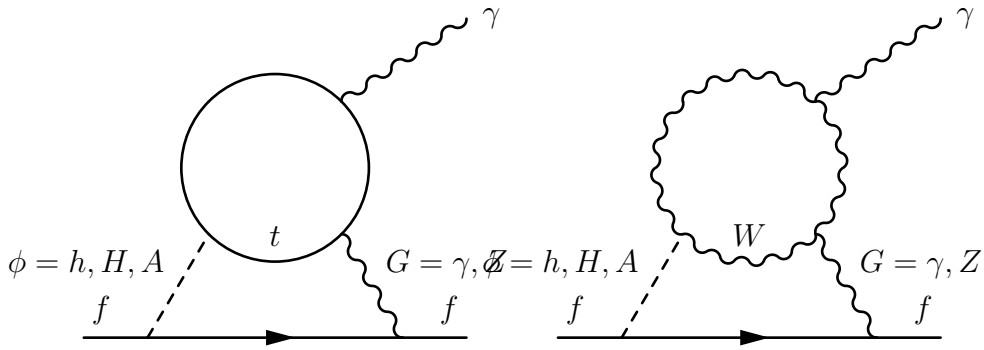


(a) Neutral Higgs, top loop




(b) Neutral Higgs, $W$ loop

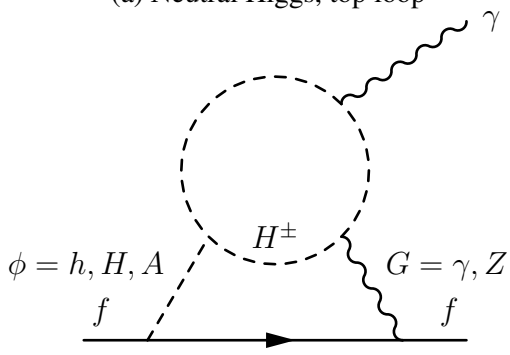


(c) Neutral Higgs, charged Higgs loop

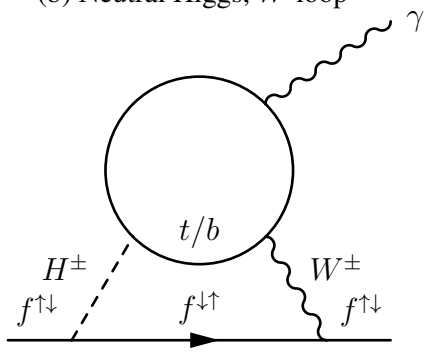


(d) Charged Higgs, top/bottom loop

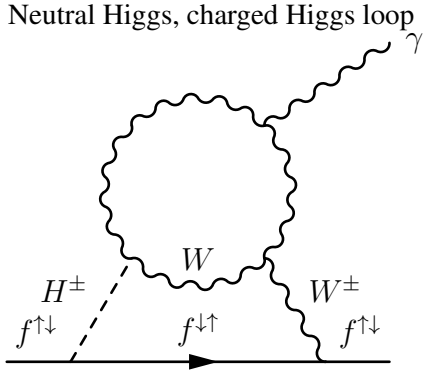


(e) Charged Higgs, $W$ loop

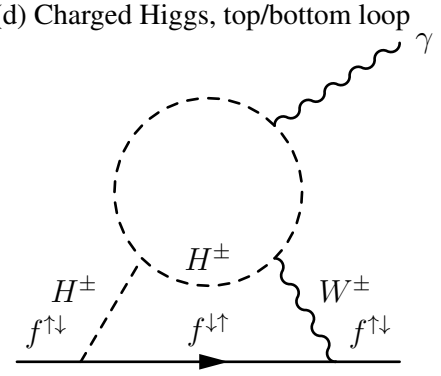


(f) Charged Higgs, charged Higgs loop

Figure 3.3: Specific Two-loop Barr-Zee diagrams

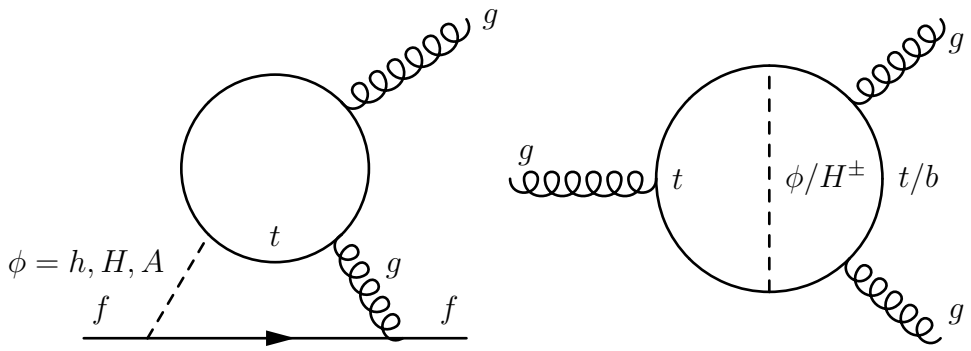


(a) Barr-Zee diagram, gluons (b) Weinberg diagram

Figure 3.4: Diagrams relevant to chromo-EDM

# Chapter 4

# Electric Dipole Moment of Leptons

Naturally, following the framework laid out previously, we want to perform EDM calculations on the various leptons.

## 4.1 Experimental Overview

A brief review of past experimental results is given in Table **??**.

| Lepton | EDM ($e\,\mathrm{cm}$) | Experime |
|---|---|---|
| $e$ | $\lvert d_e\rvert < 4.1 \times 10^{-30}$ | JILA 2023 |

As can be seen in the table, the experimental development of electron EDM (eEDM) over the past few years has been remarkably rapid. Just earlier last year, JILA [**?**] has surpassed the previous bound from ACME [**?**] and pushed the precision of eEDM down to $|d_e| < 4.1 \times 10^{-30}\, e\,\mathrm{cm}$. It is noteworthy to point out that these eEDM experiments are relatively small in scale, "tabletop experiments" even when compared to behemoths like the LHC, which makes the extreme precision achieved all the more impressive.

## 4.2 The Electron

For the electron, an extensive study of eEDM in G2HDM can be found in the 2018 and 2020 papers of Fuyuto, Hou, and Senaha (Refs. [**?**]). Our investigation on eEDM is essentially an extension of the 2020 paper to a larger parameter space.

### 4.2.1 Cancellation Mechanism

As mentioned in [CROSSREF], one big motivation for G2HDM as a viable model is the fact that $\mathcal{O}(1)\rho_{tt}$ can drive baryogenesis through $\lambda_t \mathrm{Im}\rho_{tt}$. However, this same $\rho_{tt}$, along with $\rho_{ff}$ for a given fermion $f$, also generates EDM for said fermion [CROSSREF]. We thus arive at a "point of tension" between theory and experiment: we desire a large $\rho_{tt}$ for baryogenesis, but need a small $\rho_{tt}$ to survive precision bounds on various EDMs. Electron EDM, in particular, is a great "observable of contention", since experiments measuring it are the most precise compared to other EDMs. In an attempt to address this issue, Fuyuto, Hou, and Senaha proposed a "cancellation ansatz" between $\rho_{ee}$ and $\rho_{tt}$

$$\mathrm{Re}\rho_{ee} = -r\frac{\lambda_e}{\lambda_t}\mathrm{Re}\rho_{tt}, \quad \mathrm{Im}\rho_{ee} = +r\frac{\lambda_e}{\lambda_t}\mathrm{Im}\rho_{tt}, \tag{4.1}$$

which facilitates a "cancellation mechanism" that allows for small values of eEDM while keeping a *sizeable* $\rho_{tt}$. The "cancellation" in this mechanism arises from the opposite signs of the $W$-loop and the top-loop in the Barr-Zee diagrams. Referring to (**??**) and (**??**), we can see that

$$(d_l^{\phi G})_t = -\frac{e\, m_l}{(4\pi)^4}\sqrt{2}G_F \sum_{\phi=h,H,A}\sum_{G=\gamma,Z}(\rho \text{ couplings})(\text{Loop functions}) \tag{4.2}$$

$$(d_l^{\phi G})_W = +\frac{e\, m_l}{(4\pi)^4}\sqrt{2}G_F \sum_{\phi=h,H,A}\sum_{G=\gamma,Z}(\rho \text{ couplings})(\text{Loop functions}) \tag{4.3}$$

thus the effectiveness of such a cancellation is determined by the relationship between the new $\rho$ couplings and the loop functions of the Barr-Zee diagrams. In the case of total cancellation, $(d_l^{\phi G})_t = -(d_l^{\phi G})_W$, which gives

$$\text{To be added} \tag{4.4}$$

which can be factored into a $\rho$-dependent part and a loop-function-dependent part $r$. Rearranging (**??**) thus gives us the form of the cancellation ansatz. This ansatz signifies two key points. First, it gives a flavor hierarchy $|\rho_{ee}|/|\rho_{tt}| \sim \lambda_e/\lambda_t$ that reflects SM. Second, it represents a phase lock between $\rho_{ee}$ and $\rho_{tt}$. With our working assumption of Higgs masses, this ansatz results in a "dip" in eEDM around the $r$ value of $\sim 0.7$, which is when complete cancellation occurs between the $W$-loop and the top-loop. This provides a mechanism for the eEDM in G2HDM to be small and evade the experimental bounds while not directly modifying $\rho_{tt}$.

### 4.2.2 Enlarging the Parameter Space

When revisiting their study, we found the assumptions on the value of $\rho_{tt}$ to be quite "conservative", setting $\mathrm{Re}\rho_{tt} = \mathrm{Im}\rho_{tt} = -0.1$ (which equates to $|\rho_{tt}| = 0.1\sqrt{2} \approx 0.14$). We believe that might be due to *playing it safe* under the pressure of the rapid advancements on the experimental front. In our study [**?**], we *push against the boundary*, and explore a larger range of $\rho_{tt}$, up to $\mathrm{Re}\rho_{tt} = \mathrm{Im}\rho_{tt} = -0.3$ ($|\rho_{tt}| = 0.3\sqrt{2} \approx 0.42$). We want to see how big we can keep the parameter space for baryogenesis while still satisfying precision constraints. As mentioned before, one of the key points of G2HDM is the *flavor hierarchy*, illustrated by the *rule of thumb* (2.2). This "cancellation ansatz" happens to capture the idea of such a hierarchy pretty well from a numerical standpoint; so, for the sake of numerical illustration of the flavor hierarchy, we extend the ansatz to all fermion $\rho_{ff}$s, except for the top itself:

$$\mathrm{Re}\rho_{ff} = -r\frac{\lambda_f}{\lambda_t}\mathrm{Re}\rho_{tt}, \quad \mathrm{Im}\rho_{ff} = +r\frac{\lambda_f}{\lambda_t}\mathrm{Im}\rho_{tt}. \tag{4.5}$$

We must reiterate that this is merely a move of convenience, and the actual values of the $\rho_{ff}$s need not precisely match this ansatz. Results are shown in Figure 4.1.

For the sake of clarity, we have taken a slight liberty in illustrating the range of the purple "allowed window" band, using the left- and right-most curves instead of the left and right side of a given curve. Nevertheless, the trend we wish to describe

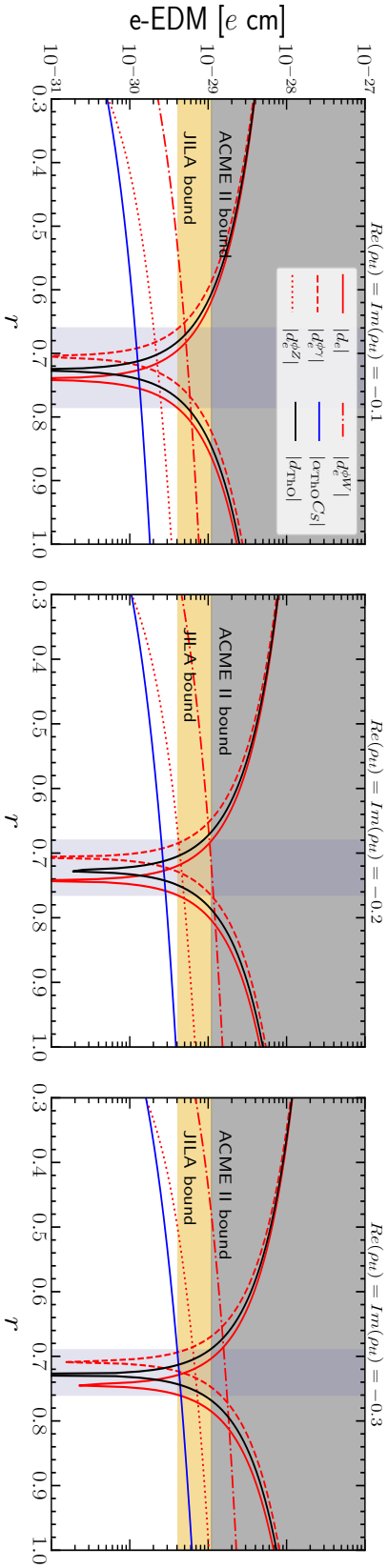


Figure 4.1: eEDM v.s. $r$ for a larger range of $\rho_{tt}$ with ansatz Eq. (4.5). ($c_\gamma = 0.1, m_{H,A,H^+} = 500\,\text{GeV}$)

is not affected by such. From our results, it can be seen that as $|\rho_{tt}|$ increases, the allowed window of the proportionality parameter $r$ shrinks, yet there is still a decent range of acceptable probable values. $\mathrm{Re}\rho_{tt} = \mathrm{Im}\rho_{tt} = -0.1$ was indeed a conservative representative value, and $\mathrm{Re}\rho_{tt} = \mathrm{Im}\rho_{tt} = -0.3$ may still be a viable option in the baryogenesis parameter space.

## 4.3 The Muon

After the electron, we move on to its slightly heavier cousin, the muon. Since the bound on the muon is not as strong, one does not need to resort to the cancellation ansatz immediately. Instead, we perform a scan of the $\rho_{tt}$ parameter space for a representative $\rho_{\mu\mu}$ value, and see how it affects the $\mu$EDM. Results are shown in Figure 4.2.

We see that there is still a "cancellation dip" for the neutral scalar-attached loops, which arises from the opposite signs of the $W$-loop and the top-loop. The details of said cancellation is exactly the same as that of the electron. Our predicted values for $\mu$EDM are still two to three orders of magnitude below the current bounds, so we are eager to see development on the experimental front. Once the bounds close in, it may also be fruitful to consider the "cancellation ansatz" on the muon as well, especially since the leptons share a extra Yukawa matrix $\rho^l$, which makes it more likely that the $\rho_{ll}$ might exhibit similar relationships with $\rho_{tt}$.

## 4.4 The Tau Lepton

Lastly, we analyze the heaviest lepton, the tau. On the experimental front, the precision of tau EDM ($\tau$EDM) measurements are still pretty low. We perform the same calculations as the muon, with $\rho_{\mu\mu} = i\lambda_\mu$ replaced by $\rho_{\tau\tau} = i\lambda_\tau$. Results are shown in Figure 4.3. As seen in the figure, our predicted values are still several orders of magnitude below current experimental results. Further precision

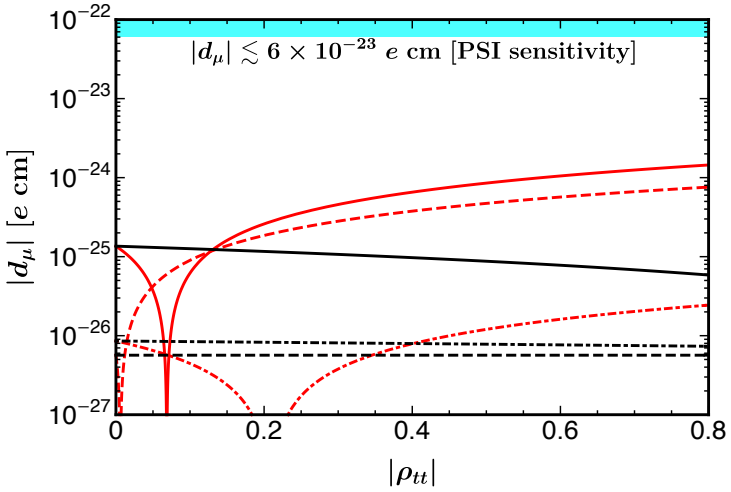


Figure 4.2: $\mu$EDM results.

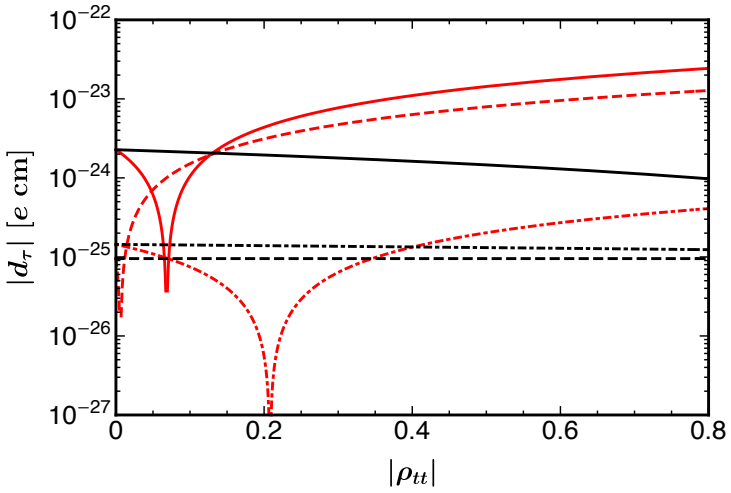


Figure 4.3: $\tau$EDM results.

or methodology improvements are required for a more fruitful analysis of $\tau$EDM, so we just present our results here without much further comment.

# Chapter 5

# Electric and Chromo-electric Dipole Moment of Quarks

After the analysis for leptons, we turn our gaze towards EDMs involving quarks. As mentioned in the theory section, there are additional chromo-EDM and Weinberg term contributions to take into account that arise from the fact that quarks interact via QCD. However, since quarks are always confined as hadrons, it is extremely difficult, if not outright impossible, to directly probe the EDMs of individual quarks, given the state of current technology and our understanding of QCD. A quick literature review shows that there are indeed no direct experimental observations for the EDMs of all the quarks lighter than the top quark. As for the top quark, there has been experimental progress at CMS to constrain the value of its chromo-EDM, as seen in Refs. [**?**] and [**?**]. This, in fact, was our original motivation for exploring quark EDMs in G2HDM. Alas, the constraints imposed by the aforementioned analyses are still relatively weak, so we do not pursue this observable any further for the moment. We do want to keep an eye out for further experimental developments on this front, though. It is natural, under these circumstances, to shift our attention towards hadron EDMs, and utilize the EDM of hadrons to observe the effect of the EDMs of individual quarks. The prime candidate in this case would be the neutron EDM (nEDM).

Neutron EDM measurements have been in the experimental realm for quite some time already. The most recent results are given by PSI [**?**] in 2020, setting the bound at $|d_n| < 1.8 \times 10^{-26}\ e\,\mathrm{cm}$. A recent report from the Snowmass conference [**?**] has shed some light on the past, present, and future of nEDM experiments. As can be seen from Figure 5.1 taken from said report [**?**], progress on the nEDM front has stagnated for a decade or so, with the precision plateauing at $\sim 10^{-26}\ e\,\mathrm{cm}$. However, projects to improve the sensitivity are already in the works, so it is still worth to explore the nEDM parameter space.

We use the recent formula [**?**]

$$d_n = -0.20\, d_u + 0.78\, d_d + e\,(0.29\, \tilde{d}_u + 0.59 \tilde{d}_d) + e\, 23\ \mathrm{MeV}\, C_W \tag{5.1}$$

to estimate the nEDM. We evaluate the contributions to $\tilde{d}_{u,d}$ and $C_W$ in G2HDM by following Refs. [**?**] and [**?**], with discussion on theoretical uncertainties found in Ref. [**?**]. We present the results for nEDM in Figure 5.2, as well as combined results for eEDM and nEDM in the range $r \in [0.6, 0.8]$ in Figure 5.3, with the "extended" ansatz (4.1) applied.

Interestingly, our predictions for nEDM are not too far below the current experimental bound. We see that, even for $|\rho_{tt}| = 0.3\sqrt{2} \approx 0.42$, one can still survive the current PSI bound. In the combined plot, the eEDM cancellation mechanism from the previous section at $r \approx 0.7$ clearly illustrated. The interplay of the nEDM and the eEDM in Figure 5.3 shows that our predictions are of notable significance in both precision observables. The follow-up project at PSI, named n2EDM [**?**], plans to reach a sensitivity of $\sim 10^{-27}\ e\,\mathrm{cm}$ within a decade, which covers the range illustrated in Figure 5.2.

We have been utilizing the "extended" cancellation ansatz (4.1) in our above calculations and analyses, but we have to stress that, as described before, it is merely a convenient way to numerically illustrate the *flavor hierarchy* of the G2HDM. A closer examination of the "extended" ansatz reveals a logical flaw: since $\rho_{uu}$ and $\rho_{tt}$ are in the same $\rho$ matrix, and the ansatz obviously does not hold for $\rho_{tt}$ itself, there is no reason to expect it to hold for $\rho_{uu}$. Thus, for this situation, we should

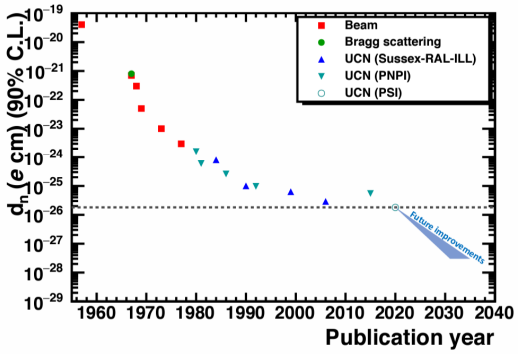


Figure 5.1: nEDM experimental progress [**?**]

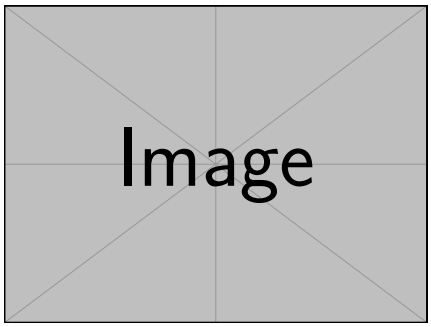


Figure 5.2: nEDM results.

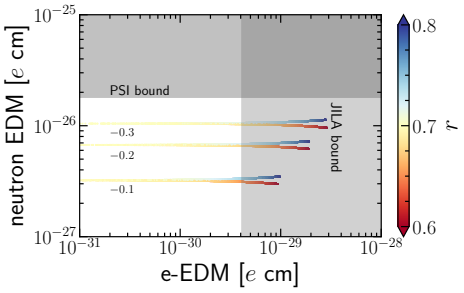


Figure 5.3: Combined eEDM-nEDM result.

fall back one step, and rely on the *rule of thumb* (2.2) instead of the ansatz. Hence, we relax the ansatz for $\rho_{uu}$, and explore the range of $\mathcal{O}(\lambda_u)$ by varying

$$|\rho_{uu}| \in [0.3\lambda_u, 3\lambda_u], \quad \arg \rho_{uu} \in [-\pi, \pi] \tag{5.2}$$

while keeping the other $\rho_{ff}$s intact, i.e. still following the ansatz. We present our results in Figure 5.4.

The different colors of the points represent different values of $\arg \rho_{uu}$, and an interesting pattern can be seen among them. The red points have negative $\arg \rho_{uu}$, which is the same sign as $\rho_{tt}$; the nEDM of these points are larger, but stay mostly below the PSI bound. On the other hand, the blue points have *positive* $\arg \rho_{uu}$, which is the *opposite* sign as $\rho_{tt}$; remarkably, the value of nEDM of these points drop significantly, reaching as low as $10^{-28}\ e\,\mathrm{cm}$ or lower, evading even the projected sensitivity of n2EDM at PSI! This phenomenon in Figure 5.4 illustrates a *natural* cancellation mechanism present within the dynamics of nEDM, arising from the phase difference of $\rho_{uu}$ and the other $\rho_{ff}$. Even though this mechanism can evade the projected n2EDM sensitivity, it can still be probed by future experiments, such as the Spallation Neutron Source (SNS) at Oak Ridge National Laboratory (ORNL) [**?**], which can reach sensitivities down to $\sim 10^{-28}$ $e\,\mathrm{cm}$. This experiment may take more than a decade to come to fruition, but it almost fully covers our projected range, since the blue dots are still mostly concentrated above $10^{-28}\ e\,\mathrm{cm}$.

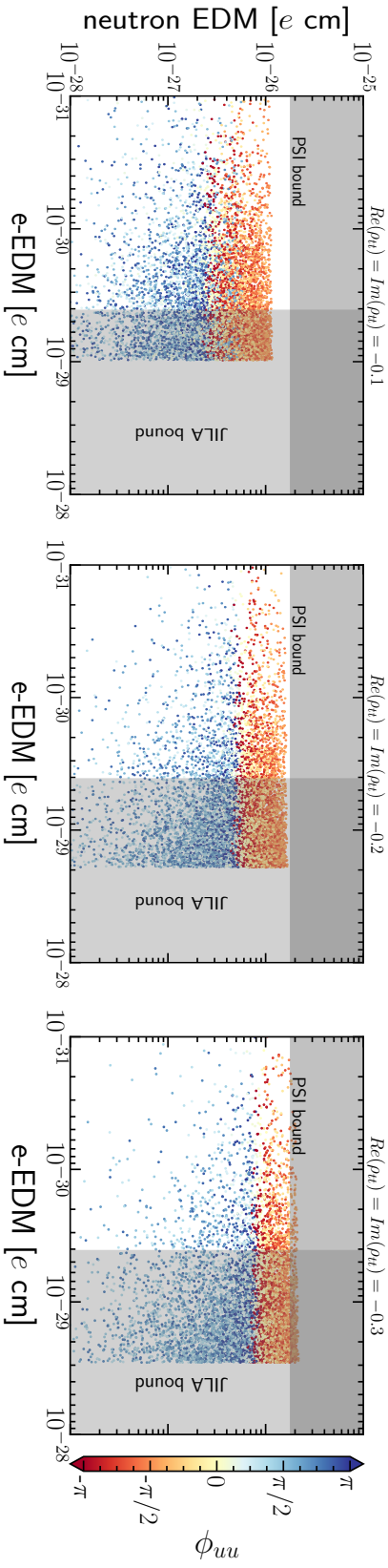


Figure 5.4: Results for eEDM and nEDM with $|\rho_{uu}| \sim \lambda_u$.

# Chapter 6

# Conclusion

## 6.1 Comments

Before we reach the summary of this study, we want to comment on some unaddressed details.

### 6.1.1 Heavy Higgs Masses

Throughout the calculations in this study, we have assumed degeneracy of the exotic Higgses, either at 300 or 500 GeV. This has been done primarily to reduce the number of variables in the analysis, and focus on the effects of the extra Yukawa couplings on various EDMs. As a matter of fact, this assumption is actually two assumptions in one: the choice of benchmark mass value and the choice of imposing degeneracy. We would like to address the concequences of lifting/flexing each assumption seprately. First, regarding the choice of benchmark. For eEDM and nEDM, we have set the exotic Higgs masses to the higher value of 500 GeV. This leads to a smaller two-loop contribution to the EDMs, since the loop functions are dependent on and monotonically increasing with $m^2_{t/W}/m^2_{H/A/H^+}$. This also changes the exact $r$ value where the cancellation occurs. However, at the same time, larger exotic Higgs masses lead to a less efficient scenario for baryogenesis. In a sense, this is the "conservative" benchmark, sacrificing baryogenesis efficiency

for some extra "headroom" in evading the EDM bounds. On the other hand, the 300 GeV mass value used in the $\mu$EDM and $\tau$EDM calculations is the "optimistic" benchmark, meant to explore the upper limits of the respective EDMs and see how close we are to the current experimental bounds. We have checked the eEDM and nEDM calculations at the 300 GeV benchmark and, unsurprisingly, the qualitative results are the same, with only the quantitative differences described above. Second, regarding the mass degeneracy. As mentioned in [CROSSREF], with the degeneracy in place, one-loop effects are even further supressed. Lifting this degeneracy will increase the importance of the one-loop contribution, but unless the off-diagonal terms of the lepton $\rho$-matrix are large, which runs against our *flavor hierarchy* phenomenon, the two-loop effects will still be dominant by at least an order of magnitude or two. Also, nondegenerate exotic Higgs masses opens us up to the scrutiny of electroweak precision constraints [**?**]. This will require us to explore the scenarios of custodial symmetry $m_A = m_{H^+}$ and twisted-custodial symmetry [**?**] $m_H = m_{H^+}$. All in all, we can still enlarge the parameter space by varying the masses of the exotic Higgses, but we will have to deal with different constraints. We thus relegate a thorough investigation of the Higgs masses to further studies.

### 6.1.2 Muon $g - 2$

### 6.1.3 Top Chromo-EDM

We would like to mention that the nEDM portion of this study was originally motivated by the ability of the LHC to probe top CPV through top chromo-EDM [**?**]. Probing the EDM and cEDM of the top quark directly would be ideal for direct exploration of the $\rho_{tt}$ parameter space. Alas, the current bounds of the top cEDM are still relatively weak, so we shifted our gaze towards other hadronic EDMs and settled on nEDM, where the up and down cEDM come into play. Fortunately, we found rather good prospects for G2HDM in nEDM! We do hope that future

improvements on the top cEDM measurement will come to fruition, and eagerly anticipate the insights it may bring in the realm of CP violation.

## 6.2 Summary and Conclusion

We present an analysis of various EDMs of fundamental particles in the framework of a G2HDM. We note that to evade precision bounds while satisfying the conditions for baryogenesis, a cancellation is possible, which is also an indicator of an underlying *flavor hierarchy*. This is most prevalent in eEDM, where bounds are the strongest, and experimental precision improving rapidly. We analyze $\mu$EDM, with our predictions still being a couple orders of magnitude below current experimental bounds. We present results for $\tau$EDM, but provide no further analysis since the bounds are still too imprecise. We analyze quark EDM through nEDM, and optain promising prospective results, especially when viewed together with eEDM. We stress that this is a noteworthy area to pay attention to in the upcoming decade or two.

# Reference